Research article

Viacheslav I. Korolev, Anatoly P. Pushkarev, Petr A. Obraztsov, Anton N. Tsypkin, Anvar A. Zakhidov and Sergey V. Makarov*

Enhanced terahertz emission from imprinted halide perovskite nanostructures

https://doi.org/10.1515/nanoph-2019-0377
Received September 20, 2019; revised November 18, 2019; accepted November 27, 2019

Abstract: Lead halide perovskites were known to be a prospective family of materials for terahertz (THz) generation. On the other hand, perovskite nanostructures, nanoantennas, and metasurfaces allow tailoring perovskites optical characteristics, resulting in more efficient interaction with incident or emitted light. Moreover, the perovskites are robust materials against formation of defects caused by mechanical deformations and can be efficiently nanostructured by various high throughput methods. In this work, we have enhanced THz emission from $MAPbI_3$ perovskite upon femtosecond laser irradiation using nanoimprint lithography. The formed nanostructures not only improve absorption of the incident laser pulses, but also lead to a non-symmetric near-field distribution. As a result, we have enhanced the efficiency of THz emission from the nanostructured perovskite by 3.5 times as compared with a smooth perovskite film. Our results paved the way for a new application of large-scale perovskite nanostructuring, making halide perovskites competitive with more expensive conventional semiconductors for THz generation.

Keywords: halide perovskites; nanostructures; nanophotonics; nanoimprint lithography; THz generation.

***Corresponding author: Sergey V. Makarov,** ITMO University, St. Petersburg, 197101, Russia, e-mail: s.makarov@metalab.ifmo.ru. https://orcid.org/0000-0002-9257-6183
Viacheslav I. Korolev, Anatoly P. Pushkarev and Anton N. Tsypkin: ITMO University, St. Petersburg, Russia
Petr A. Obraztsov: ITMO University, St. Petersburg, Russia; and Prokhorov General Physics Institute, Russian Academy of Sciences, Moscow 119991, Russia
Anvar A. Zakhidov: ITMO University, St. Petersburg, Russia; and University of Texas at Dallas, Richardson, TX 75080, USA

1 Introduction

Methylammonium lead iodide perovskite ($CH_3NH_3PbI_3$ or $MAPbI_3$) is an organic-inorganic material, which combines vital advantages for modern photonic sources [1], optoelectronics, [2] and photovoltaics [3], such as strong direct interband transitions resulting in high absorption in visible range ($\alpha > 10^5$ cm^{-1}) and efficient luminescence, whereas huge carrier lifetimes (up to microsecond scale) yield long carrier diffusion lengths [4]. Moreover, it is a solution processed semiconductor and thin films are formed at low temperatures considerably to simplify functional devices fabrication.

Recently, this material was proposed as a novel and relatively efficient source of terahertz (THz) emission after pumping it above bandgap with femtosecond laser pulse [5–7]. Photo-Dember [5], bulk photovoltaic [6], and surface depletion field [7] effects were proposed to be main mechanisms responsible for the THz generation in $MAPbI_3$. Also, the generation of THz radiation from lead bromide perovskite due to shift current mechanism upon two-photon nonlinear excitation was demonstrated very recently [8]. Despite the exact physical origin and contribution of different effects to the process of THz emission in perovskites, it is still the field of debates. Relatively efficient emission of THz radiation was recently demonstrated with the electric field amplitude only one order of magnitude lower than that of InAs [7], paving the way for creation of cheap, compact, and efficient THz sources.

Further optimization of the THz emission efficiency can be done by employing advanced nanophotonic structures, as it was achieved with various semiconductors [9–16]. In turn, halide perovskite nanophotonics [17, 18] and metaoptics [19] are rapidly developing platforms for boosting efficiencies of various optical and optoelectronic devices from lasers to solar cells. In particular, periodic arrays of perovskite nanostructures were employed for luminescence enhancement [20–23], solar cells efficiency improvement [24], and optimization of light outcoupling from perovskite light emitting devices

[25]. Halide perovskite integrated with various plasmonic structures were also employed for efficient THz pulses modulation [26–29]. Moreover, halide perovskites are soft enough to enable nanoimprint lithography (NIL), being one of the most throughput method for perovskite functional patterning [30], which is hard to exploit for conventional semiconductors (e.g. III–V compounds) that are the most efficient sources of THz.

In this work, we proposed an approach to enhance THz emission from a halide perovskite thin film by means of its nanopatterning. We showed experimentally that THz field amplitude can be enhanced up to 1.75 times (or up to 3.5 times for THz intensity) with strong dependence on polarization of the incident light. Our numerical simulations show that the nanostructure supports lateral gradients for near-field in the sub-surface layer making the contribution stronger to THz generation via free carriers transient spatial separation. The applied NIL approach for the perovskites nanopatterning paves the way for cost-efficient THz emitters fabrication.

2 Methods

2.1 Perovskite synthesis

Lead(II) iodide (PbI_2, 99.99%, TCI), methylammonium iodide (MAI, 99.8%, Dyesol), dimethylsulfoxide (DMSO, 99.8%, anhydrous, Alfa Aesar), N, N-dimethylformamide (DMF, 99.8%, anhydrous, Sigma-Aldrich), diethyl ether (95%, Vecton) were used as received. PbI_2 (1 mmol, 461 mg) and MAI (1 mmol, 159 mg) were mixed and dissolved in DMF (700 mg) and DMSO (70 mg) by shaking for 5 min to give 1.25 M perovskite precursor solution. The solution was filtered by using 0.45 μm PTFE syringe adapter. All the manipulations were carried out in a N_2-filled glove box with H_2O and O_2 levels not exceeding 1 ppm.

2.2 Thin film deposition

Glass substrates of 1.5 × 1.5 cm size were cleaned mechanically with sodium bicarbonate and after that subsequently sonicated in acetone and 2-propanol (IPA) for 5 min. Before the spin-coating, the substrates were treated with ozone for 3 min to eliminate residual surface contaminants. Then, substrates were evenly covered with 35 μl of the perovskite ink and spun for 55 s. A spin-coating procedure consisted of two steps: (i) 1000 rpm for 10 s; (ii) 2000 rpm for 45 s. One milliliter of diethyl ether was dripped on top of the precursor layer at 15 s to precipitate perovskite in the form of polycrystalline thin film. After the spin-coating, the substrates were annealed on the hot plate for 30 min at 50°C.

2.3 Nanoimprint lithography

After the annealing the samples were subjected to NIL process. As a master form a standard commercial optical DVD disk was exploited. The mold was prepared in the following way: a plastic part of a disc was separated from a part covered with metal foil; the latter was cut in 1×1 cm^2 pieces suitable for NIL procedure. At room temperature, pressure of 1 ton per 1 cm^2 was applied to the mold laying over perovskite film. In order to get high-quality grating, NIL procedure should be accomplished in a certain time window when the concentration of DMF/DMSO in $MAPbI_3$ film is small enough to avoid removal of the perovskite material from the substrate with the mold. However, the remaining solvent fraction should be sufficient for surface modification in the pressure range when the substrate does not crack.

2.4 Samples characterization

Morphology of the perovskite films before and after NIL process was studied with a scanning electron microscope (SEM, Zeiss Auriga FIB-SEM) in back-scattering electrons mode. Accelerating voltage was 5 kV to avoid perovskite damage or degradation upon the electron beam.

2.5 THz experiments

For detection of THz radiation, we used reflection geometry (the angle of incidence to the surface is equal to 45°) with phase-sensitive electrooptic sampling. As a pump source we took laser with 35 fs pulse duration, wavelength 400 nm (second harmonic generated in BBO crystal), with rate 1 kHz, the size of the beam is 0.5 cm^2. For electro-optic sampling 1 mm ZnTe crystal was employed. It should be noted that the experimental setup did not provide nitrogen purging. Experimental setup is shown in more details in Section S1 in Supporting Information.

2.6 Transient photocurrent measurements

To induce photocurrents in fabricated samples, we employed second harmonic of Ti:Sapphire amplified system output, delivering 40 fs, 2.5 mJ pulses with 1 kHz

repetition rate at 800 nm (1.55 eV) fundamental wavelength. The pump fluences used to excite the samples are well below the damage threshold of initial perovskite layer and did not result in any visible damage during the measurements. In experiments, the unfocused pump beam with diameter of 0.5 cm was directed to the sample surface at incidence angle 45°, providing fluence around 100 μJ/cm^2. The induced photocurrents were measured at room temperature and zero-bias across conductive electrodes applied to the surface of perovskite samples by the voltage drop on the 50 Ω input impedance of a 600 MHz digital oscilloscope connected to electrodes in short-circuit scheme.

2.7 Numerical simulations

Numerical simulations were performed by using frequency-domain solver in the commercial software CST Microwave Studio. Incidence of a plane wave with $\lambda = 400$ nm on a $MAPbI_3$ perovskite film [31] of a given profile was considered.

3 Results

3.1 Samples fabrication

For fabrication of the samples, we used NIL, which is one of the most throughput method of nanopatterning perovskite thin films, because a polycrystalline thin layer of $MAPbI_3$ behaves as a soft material that allowed us to work in a pressure range where the substrate does not crack [30]. Usually, lithographically-made silicon molds are employed for surface nanostructuring. However, manufacturing of such molds is a complex and expensive process, therefore, risk of damaging during NIL restrains their utilization for large-scale and mass-production applications. In order to make a nanostructure on a perovskite layer, we used a metallic part of an unrecorded commercial DVD disk, representing 1D grating with a period of 0.75 μm.

The schematic illustration of the fabrication process is shown in Figure 1A. Initially, 600-nm-thick perovskite film covers the glass substrate evenly (Figure 1B, more details on the films synthesis and deposition see Section 2 Methods), and after applying NIL, a grating with period ≈0.75 μm, line width ≈0.5 μm, and height ≈0.1 μm is formed on the film surface (Figure 1C). Also, the samples show rainbow colours under white light illumination due to light diffraction on the formed grating (Figure 1A). Such surface grating might be useful for not only standard optical applications, but also can be employed for enhanced THz emission as schematically shown in Figure 1D.

3.2 THz measurements

In order to generate THz emission from the obtained samples we irradiated them by second harmonic of 35-fs amplified Ti:Sapphire laser centered at 400 nm (for details,

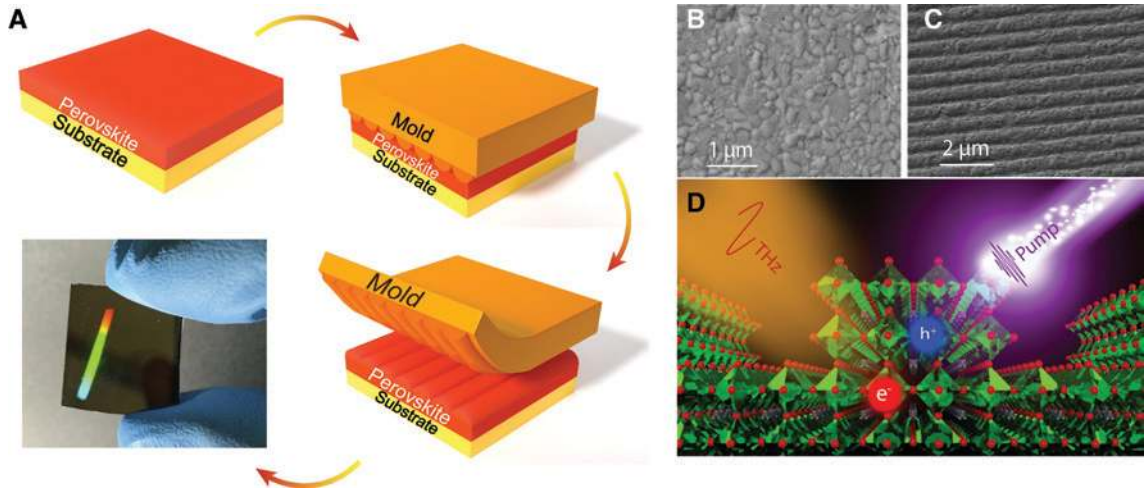

Figure 1: Samples and concept.
(A) Technological steps for nanostructured $MAPbI_3$ films fabrication by means of nanoimprint lithography (NIL). SEM images of a perovskite film before (B) and after (C) NIL. (D) Schematic illustration of the principle of THz generation enhancement in the nanostructured perovskite film (upper) as compared with a smooth film (lower).

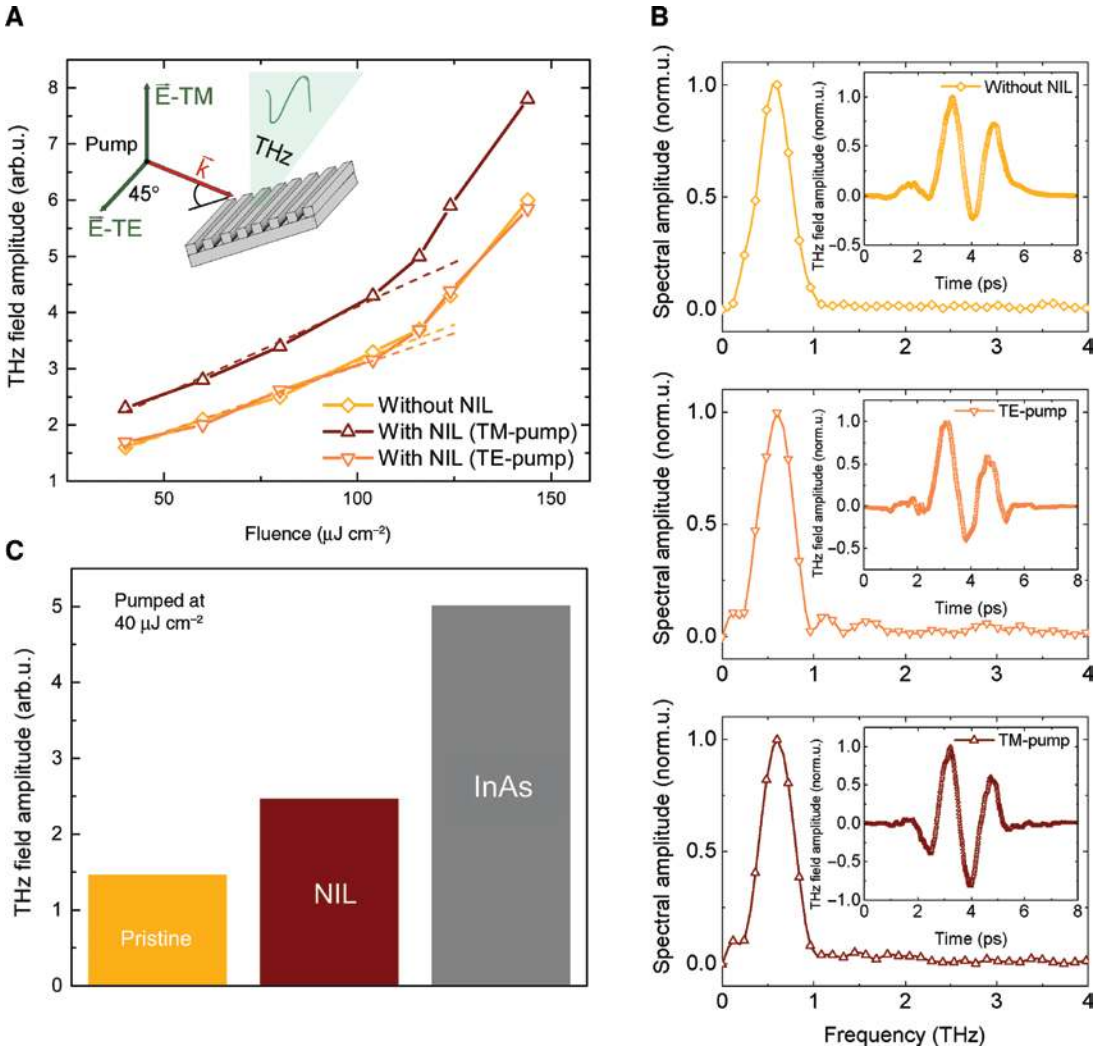

Figure 2: THz measurement results.
(A) Experimentally measured dependence of THz amplitude from smooth (yellow line) and nanoimprinted (NIL, brown and orange lines) $MAPbI_3$ films on fluence of femtosecond laser pump. (B) Spectra of the THz pulse generated from the $MAPbI_3$ films at fluence 100 μJ/cm², where the curve colors are similar to those on picture (A). (C) Comparison of THz field amplitude from smooth and nanostructured perovskite films with a commercial InAs slab.

see Methods). In agreement with previous studies [5, 7], Figure 2A shows, that the peak amplitude of the emitted THz radiation is a linear function of incident laser fluence. Deviation from the linear dependence is observed only at higher pump fluence (>100 μJ/cm²) which is close to the threshold of perovskite visible modification. Namely, at higher fluences, the THz signal is not stable and film irreversibly changes color to yellow in 10 minutes approximately, which might be related to perovskite decomposition MA.

The inset of Figure 2A shows the mutual orientation of polarization vector of the incident laser field and grooves direction. We considered two incident polarizations for the laser pulse falling on the $MAPbI_3$ film at the angle of incidence equal to 45°, i.e. when the polarization vector is parallel (TE) and perpendicular (TM) to the grooves, respectively. The insets of Figure 2B show generated THz field amplitude in time domain measured at fluence equal to 100 μJ/cm². At the time ≈1.8 ps relatively to the arbitrary chosen starting point similar for the all measurements, we observed the build up of THz emission. The maximum THz field amplitude was observed after ≈3.1 ps. The field oscillations of THz pulses can be detected until ≈6 ps. After that, we did not detect any measurable signal at the picosecond scale. To analyze spectrum of emitted THz radiation, we applied Fast Fourier Transformation. The resulting spectra are shown in Figure 2B, where central peaks of the THz emission are

located at ≈0.6 THz, which is consistent with previously reported experiments [5, 7].

We also compared THz emission from perovskite and InAs semiconductor, which predominantly generates THz via photo-Dember effect [32]. Figure 2C represents the comparison between THz field amplitudes from different samples measured in reflection configuration upon identical excitation conditions (fluence 40 μJ/cm^2). As compared to the InAs slab, the generated THz radiation is ≈3.5 times (lower) for the smooth perovskite thin film and ≈2 times lower for the nanopatterned sample pumped with TM-polarized light.

3.3 Ultrafast photocurrent measurements

In order to provide the comparison between performance of smooth and NIL perovskite layers, we performed additional photocurrent measurements. We employed the experimental procedure developed in the work [6] and have described in details in Section 2 Methods. The experimental geometry is schematically depicted in Figure 3A. Upon excitation with femtosecond pulses, the duration of the induced transient photocurrent response obtained from the perovskite sample is determined by the registration system bandwidth rather than by the internal characteristics of the sample, while its magnitude represents the time-integrated current. Since the photocurrent is triggered by an ultrashort (40 fs) laser pulse and the current dynamics in perovskite is expected to be on a sub-picosecond time scale [26, 29], the time-varying current J should result in the emission of the THz wave proportional to dJ/dt [33]. Since these photoexcitations occur in the unbiased sample, the transient photocurrents J_x and J_y or the resultant free-space emission of TE- or TM-polarized THz radiation, respectively, provides information regarding the internal bias near the sample surface.

The typical temporal profiles of photocurrent pulses induced in smooth and NIL perovskite samples under excitation with different optical polarizations are shown in Figure 3B. As one can see from Figure 3B both TE- and TM-polarizations induce pronounced photocurrent response in smooth and NIL samples. While the amplitude of photocurrent signal in smooth sample is oscillating around zero, in the case of structured sample there is pronounced enhancement of response when the polarization vector of light is perpendicular to the grooves of the imprinted grating.

By measuring the voltage drop across two orthogonal pairs of electrodes, we were able to simultaniously measure longitudinal (J_x) and transverse (J_y) components with respect to the light incidence plane components of the induced photocurrent as well as to the patterned grooves in the NIL sample. Polarization dependences of the induced J_x and J_y components of the photocurrents were identified by measuring the peak-to-peak amplitudes of the corresponding photocurrent waveform while rotating half ($\lambda/2$) waveplate positioned before the sample by an angle, which varied the state of the laser polarization with a period of 90°.

The peak amplitude values of the photocurrent signals induced in smooth and NIL perovskite films as a function of light polarization (rotation of $\lambda/2$ plate) are shown in Figure 3C and D, respectively. Generally, one can see the increased amplitude of the sinusoidal curves for NIL sample as compared with smooth one (see additional description of the measurements in Supporting

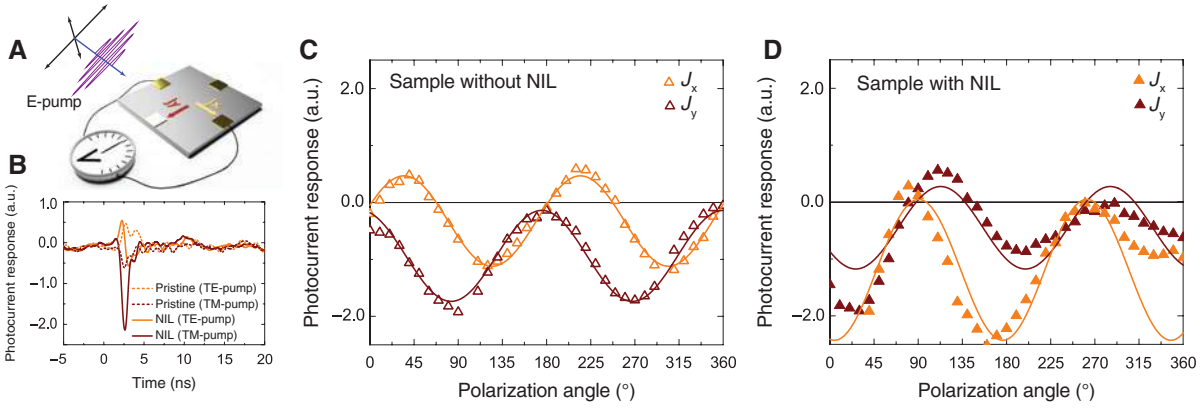

Figure 3: Photocurrent response.
(A) A scheme of the photocurrent experiment. (B) Typical temporal profiles of photocurrent pulses induced in smooth and nanoimprinted perovskite films under excitation with different optical polarizations. Changes in the photocurrent with light polarization: (C) smooth perovskite sample; (D) NIL perovskite sample.

information), which also indicates the enhancement of photocurrent in the nanostructured perovskite film.

3.4 Discussion

According to our experimental findings (Figure 2A), the peak amplitude of the emitted THz field (E_{THz}) from both smooth and nanostructured samples demonstrate linear dependence on the excitation laser fluence. This is fully consistent with most of possible mechanisms of THz emission from semiconductors involving one-photon absorption which includes photo-Dember and lateral photo-Dember [5], bulk photovoltaic [6], and surface depletion field [7] effects. Indeed, independent on the exact mechanism the amplitude of emitted THz field is proportional to the number of photogenerated carriers ($E_{THz} \sim N_{eh}$, where N_{eh} is the density of photogenerated carriers) and, therefore, in the case of one-photon, absorption is linearly dependent on the incident laser fluence. Thus, the linear dependence of THz field amplitude on the pump fluence is a common feature for THz emission via one-photon absorption and cannot be used by itself to distinguish between different mechanisms of THz emission [33].

In the previously reported work [5], the photo-Dember effect was proposed as the main contribution to the generation of terahertz radiation in $MAPbI_3$. In the photo-Dember mechanism, transient current (oscillating dipole) induced by the spatial difference in photogenerated electrons and holes concentrations, and it has the direction predominantly normal to the film surface. However, radiation of such a dipole is directed mostly along the surface which obstructs the output THz field from the sample and in the absence of factors which provide the tilt of the dipole orientation from parallel to perpendicular to the surface normal photo-Dember effect would not provide any THz signal in our experimental geometry with detection in the direction of the pump laser pulses reflection. Moreover, the Dember effect by itself cannot explain the pronounced polarization dependence clearly observed in our photocurrent experiments (Figure 3C–D).

On the other hand the bulk photovoltaic effect (BPVE) was recently proposed as the possible origin ultrafast photocurrent response and THz emission from $MAPbI_3$ [6]. In general BPVE can be considered as a second-order non-linear optical effect and therefore would demonstrate linear dependence of excitation laser fluence. The distinct feature of the BPVE is pronounced dependence of induced photocurrent direction and amplitude on polarization and helicity of pump photon. Moreover, this dependence has a complex form which encodes the symmetry and the electronic band structure features of the emitting material. However, in the current study we resolved the prominent polarization dependence only in photocurrent experiment rather then in THz emission. Therefore, the separation of contributions from various effects into the generation process is not a trivial task. We considered the possible factors tilting the emitting dipole orientation leading to THz radiation pattern having its maximum in the direction of laser pulse reflection. We would like to note here that we did not exclude joint contribution of several effects, for example via constructive or destructive contribution of bulk and surface photocurrents associated with photo-Dember, lateral photo-Dember and BPVE. In order to explain the efficient THz emission in the direction coinciding the reflection of pump light, it is necessary to consider factors increasing electron-hole pairs generation efficiency (i.e. absorption increase) or change the dipole orientation (so-called lateral photo-Dember effect [34].

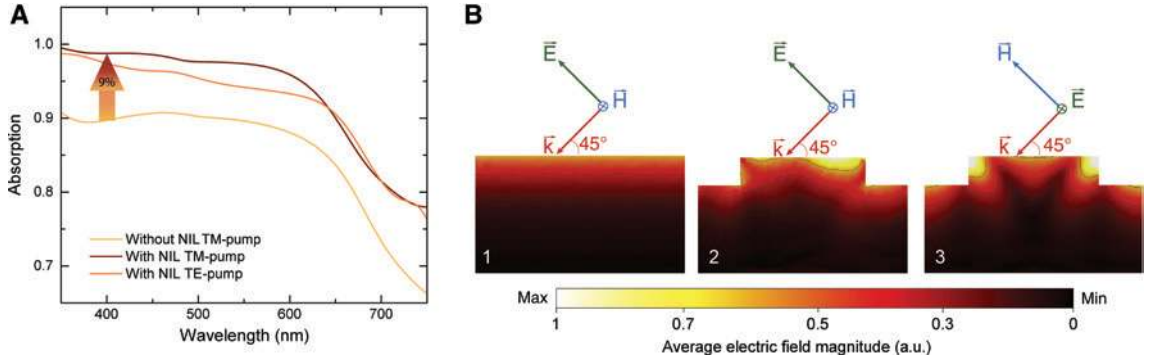

Figure 4: Calculations.
(A) Theoretically calculated absorption spectra from a flat $MAPbI_3$ perovskite film with thickness 600 nm (yellow), nanostructured film for two orthogonal polarizations of an incident light. (B) Calculated near-field distributions in the sub-surface layer of smooth (1) and nanostructured (2 and 3) $MAPbI_3$ at different polarizations (2–TM and 3–TE) of the incident light.

The contribution from increased electron-hole pairs generation in the nanostructured perovskite film can be estimated from numerical calculations of the absorption of 45° incident plane wave with wavelenght 400 nm by means of CST Microwave Studio. In Figure 4A, we have shown the resulting absorption for smooth and structured films for different orientations of the polarization of the plane wave with respect to the grooves direction. For both polarizations, the absorption for the modified samples at the wavelength of excitation increases about 8% and 9% for perpendicular and parallel polarizations, respectively. The calculated increase of absorption correlates with our additional measurements of photoluminescence and photocurrent enhancement from the smooth and nanoimprinted films (for details, see Section S2 in Supporting information). Apparently, the increased absorption itself is not sufficient to describe the 2–3.5-fold enhancement of THz intensity (E^2_{THz}), and near-field structure of the penetrated incident light has to be considered in more details.

In order to understand the effect of nanostrusturing of the $MAPbI_3$ film surface, we calculated electric-field distributions with respect to the polarization vector and morphology. The resulting images are shown in Figure 4B, where three cases are shown: smooth and nanostructured films with TE and TM polarizations of the incident light. For the smooth film, the field distribution is homogeneous with no concentration gradient along the surface, this corresponds to the movement of charges perpendicularly to the film surface. Alternatively, for the imprinted films the field distribution is not homogeneous for both polarizations. It means that the areas with local field enhancement have higher concentration of charges than rest of the regions. It induces the diffusion current in the direction where the concentration is lower. For the nanostructured samples, the near-field distribution is non-symmetric in the case of TM-polarization for 45° incident plane wave. This results in some nonzero angle relative to the surface normal for the transient current in *xy*-plane, which leads to the tilting of the induced dipole and improvement of the THz emission outcoupling. Therefore, such surface nanostructuring can improve overall efficiency of THz generation owing to both lateral photo-Dember effect and enhanced incident light absorption.

4 Conclusion

To conclude, we have demonstrated considerable enhancement of THz signal from a nanostructured $MAPbI_3$ perovskite film upon femtosecond laser irradiation. Our numerical simulations have revealed that the grating on perovskite not only improves absorption for incident laser power, but also changes the direction of diffusion current of photogenerated carriers due to non-symmetric near-field distribution. As a result, the nanoimprint lithography can be considered as one of the best approach of large scale perovskites patterning for improvement of their THz emission characteristics. Our results paved the way for new application of large-scale perovskite nanostructuring, making the halide perovskites competitive with conventional semiconductors for THz emission. Further integration with advanced photonic designs [35] and up-scaling would have a great potential for a wide range of applications from medical imaging to security screening [36].

Acknowledgement: The authors acknowledge Dr. Komissarenko for SEM measurements, and Prof. Yuri Kivshar for fruitful discussions. This work was supported by the Ministry of Education and Science of the Russian Federation (Projects 16.8939.2017/8.9 and 14.Y26.31.0010, Funder Id: http://dx.doi.org/10.13039/501100003443), for simulations and optical measurements, the Russian Science Foundation (Project 19-73-30023, Funder Id: http://dx.doi.org/10.13039/501100006769), for synthesis and characterization. P.O. is thankful to ITMO Fellowship Program.

References

[1] Quan LN, Rand BP, Friend RH, Mhaisalkar SG, Lee T-W, Sargent EH. Perovskites for next-generation optical sources. Chem Rev 2019;119:7444–77.
[2] Zhao Y, Zhu K. Organic–inorganic hybrid lead halide perovskites for optoelectronic and electronic applications. Chem Soc Rev 2016;45:655–89.
[3] Nayak PK, Mahesh S, Snaith HJ Cahen D. Photovoltaic solar cell technologies: analysing the state of the art. Nat Rev Mat 2019;4:269.
[4] Stranks SD, Eperon GE, Grancini G, et al. Electron-hole diffusion lengths exceeding 1 micrometer in an organometal trihalide perovskite absorber. Science 2013;342:341–4.
[5] Guzelturk B, Belisle RA, Smith MD, et al. Terahertz emission from hybrid perovskites driven by ultrafast charge separation and strong electron–phonon coupling. Adv Mat 2018;30:1704737.
[6] Obraztsov PA, Lyashenko D, Chizhov PA, et al. Ultrafast zero-bias photocurrent and terahertz emission in hybrid perovskites. Commun Phys 2018;1:14.
[7] Ponseca Jr CS, Arlauskas A, Yu H, et al. Pulsed terahertz emission from solution-processed lead iodide perovskite films. ACS Photon 2019;6:1175–81.
[8] He Y, Su R, Huang Y, et al. High-order shift current induced terahertz emission from inorganic cesium bromine lead perovskite engendered by two-photon absorption. Adv Functl Mat 2019;4:1904694.

[9] Seo M, Park H, Koo S, et al. Terahertz field enhancement by a metallic nano slit operating beyond the skin-depth limit. Nat Photon 2009;3:152.
[10] Park S-G, Jin KH, Yi M, Ye JC, Ahn J, Jeong K-H. Enhancement of terahertz pulse emission by optical nanoantenna. ACS Nano 2012;6:2026–31.
[11] Park S-G, Choi Y, Oh Y-J, Jeong K-H. Terahertz photoconductive antenna with metal nanoislands. Opt Exp 2012;20:25530–5.
[12] Berry CW, Wang N, Hashemi MR, Unlu M, Jarrahi M. Significant performance enhancement in photoconductive terahertz optoelectronics by incorporating plasmonic contact electrodes. Nat Commun 2013;4:1622.
[13] Jooshesh A, Smith L, Masnadi-Shirazi M, et al. Nanoplasmonics enhanced terahertz sources. Opt Expr 2014;22:27992–8001.
[14] Khiabani N, Huang Y, Garcia-Muñoz LE, Shen Y-C, Rivera-Lavado A. A novel sub-thz photomixer with nano-trapezoidal electrodes. IEEE Trans Thtz Sci Tech 2014;4:501–8.
[15] Yang S-H, Hashemi MR, Berry CW, Jarrahi M. 7.5% optical-to-terahertz conversion efficiency offered by photoconductive emitters with three-dimensional plasmonic contact electrodes. IEEE Trans Thtz Sci Tech 2014;4:575–81.
[16] Yang S-H, Jarrahi M. Frequency-tunable continuous-wave terahertz sources based on gaas plasmonic photomixers. Appl Phy Lett 2015;107:131111.
[17] Makarov S, Furasova A, Tiguntseva E, Hemmetter A. Berestennikov A, Pushkarev A. Zakhidov A. Kivshar Y. Halide-perovskite resonant nanophotonics. Adv Opt Mater 2019;7:1800784.
[18] Zhang Y, Lim C-K, Dai Z, et al. Photonics and optoelectronics using nano-structured hybrid perovskite media and their optical cavities. Phys Repo 2019;795:1–51.
[19] Berestennikov AS, Voroshilov PM, Makarov SV, Kivshar YS. Active meta-optics and nanophotonics with halide perovskites. Appl Phys Rev 2019;6:031307.
[20] Gholipour B, Adamo G, Cortecchia D, et al. Organometallic perovskite metasurfaces. Adv Mat 2017;29:1604268.
[21] Makarov SV, Milichko V, Ushakova EV, et al. Multifold emission enhancement in nanoimprinted hybrid perovskite metasurfaces. ACS Photon 2017;4:728–735.
[22] Gao Y, Huang C, Hao C, et al. Lead halide perovskite nanostructures for dynamic color display. ACS Nano 2018;12:8847–54.
[23] Zhang C, Xiao S, Wang Y, et al. Lead halide perovskite-based dynamic metasurfaces. Las Photon Rev 2019;13:1900079.
[24] Deng K, Liu Z, Wang M, Li L. Nanoimprinted grating-embedded perovskite solar cells with improved light management. Adv Funct Mater 2019;29:1900830.
[25] Shen Y, Cheng L-P, Li Y-Q, et al. High-efficiency perovskite light-emitting diodes with synergetic outcoupling enhancement. Advan Mater 2019;31:1901517.
[26] Manjappa M, Srivastava YK, Solanki A, Kumar A, Sum TC, Singh R. Hybrid lead halide perovskites for ultrasensitive photoactive switching in terahertz metamaterial devices. Adv Mater 2017;29:1605881.
[27] Chanana A, Zhai Y, Baniya S, Zhang C, Vardeny ZV, Nahata A. Colour selective control of terahertz radiation using two-dimensional hybrid organic inorganic lead-trihalide perovskites. Nat Commun 2017;8:1328.
[28] Cong L, Srivastava YK, Solanki A, Sum TC, Singh R. Perovskite as a platform for active flexible metaphotonic devices. ACS Photon 2017;4:1595–601.
[29] Chanana A, Liu X, Zhang C, Vardeny ZV, Nahata A. Ultrafast frequency-agile terahertz devices using methylammonium lead halide perovskites. Sci Adv 2018;4:eaar7353.
[30] Wang H, Haroldson R, Balachandran B, et al. Nanoimprinted perovskite nanograting photodetector with improved efficiency. ACS Nano 2016;10:10921–8.
[31] Phillips LJ, Rashed AM, Treharne RE, et al. Dispersion relation data for methylammonium lead triiodide perovskite deposited on a (100) silicon wafer using a two-step vapour-phase reaction process. Data In Brief 2015;5:926–8.
[32] Lewis RA. A review of terahertz sources. J Phys D: Appl Phys 2014;47:374001.
[33] Huang Y, Yao Z, He C, et al. Terahertz surface and interface emission spectroscopy for advanced materials. J Phys: Cond Mat 2019;31:153001.
[34] Klatt G, Hilser F, Qiao W, et al. Terahertz emission from lateral photo-dember currents. Opt Exp 2010;18:4939–47.
[35] Chen H-T, O'Hara JF, Azad AK, Taylor AJ. Manipulation of terahertz radiation using metamaterials. LPhoton Rev 2011;5:513–33.
[36] Jepsen PU, Cooke DG, Koch M. Terahertz spectroscopy and imaging–modern techniques and applications. Las Photon Rev 2011;5:124–66.

Supplementary Material: The online version of this article offers supplementary material (https://doi.org/10.1515/nanoph-2019-0377).